Optimization of Phase-Engineered

a-Si:H- Based Multijunction Solar Cells

Center for Thin Film Devices
The Pennsylvania State University
University Park, PA 16802

C. R. Wronski, R. W. Collins*,

J. Deng, X. Niu, M. L. Albert, C. Chen*, N. Podraza*

* Currently at Department of Physics and Astronomy
University of Toledo, Toledo, OH 43606

Table of Contents

Executive Summary

1. Materials Research and Device Development

RTSE has been applied to analyze growth processes for $a\text{-Si}_{1-x}\text{Ge}_x\text{:H}$ thin films, providing insights into optimization of this material as the bottom cell i-layer in triple-junction devices. Two types of excursions in parameter space were explored starting from the optimized set of conditions adopted previously for a-Si:H, i.e., 200°C, lowest power, and low reactive gas partial pressure. These excursions were designed to obtain the smoothest surfaces and largest ranges of surface stability in the $a\text{-Si}_{1-x}\text{Ge}_x\text{:H}$ deposition process. Modest improvements in surface stability were achieved with increasing temperature to ~300°C; however, major improvements were made at 200°C by altering the deposition electrode from anode to cathode. In the future, effects of controlled low energy ions, alternating growth and hydrogenation, and plasma excitation frequency are to be investigated as well as the opto-electronic properties of sufficiently thick homogeneous films.

2. Device Loss Mechanisms

The studies on identifying and characterizing the loss mechanisms in high performance cells have been continued. It is shown that from the J_D-V characteristics it is possible to identify and quantify the limitation imposed on 1 sun V_{oc} by bulk recombination. As a consequence, it is possible to relate the light induced changes in J_D-V characteristics to those in 1 sun V_{oc} for cells with undiluted and diluted protocrystalline i-layers. In addition, the new approach in the analysis of J_D-V characteristics in terms of differential diode quality factor n(V) has allowed these differences to be directly related to those in the distributions of gap states in the corresponding i-layers. The results further illustrate the serious limitations of attempts to correlate solar cell characteristics with neutral dangling bond densities, subgap absorption characterized at arbitrarily chosen photon energies or just valence band tails. They also demonstrate that J_D-V characteristics offer a *new and powerful probe* for characterizing mechanisms limiting the performance and stability of a-Si:H solar cells as well obtaining direct information about the distribution of gap states in the intrinsic layers. This is being currently applied in the characterization of USSC materials and cells. Also, kinetics of the creation and relaxation of metastable defects in i-layers of solar cells with far forward biases equivalent to high intensity illumination are being under investigation.

3. Characterization Strategies for Advanced Materials

<u>Room temperature changes in light induced defect states created by 1 sun illumination</u>

The kinetics of the changes in the light induced defect states at room temperature after 1 sun illumination have been characterized with photocurrents on films and bulk recombination currents on corresponding solar cells. The self-consistency of the two types of results further confirms that the relaxations observed in films are indeed a bulk effect! In the course of the detailed studies on films, which required multiple experiments and annealing at 170°C for 4

hours to be carried out on the same films, a new and striking result was obtained. It is in the form of systematic changes being introduced with such cycling to the initial stages of the two-component relaxation from the "same" degraded states that are indicated by degradation kinetics and end points characterized not only by the 1 sun photocurrents but also those with low carrier generation rates. This new result suggests that not only more than one defect state is involved in the relaxation but also that their relative ratios depend on the "history" of the film. Despite these changes the longer-term relaxations follow a logarithmic type of behavior that remains the same. It was established that this relaxation is due to the changes in the gap states located around midgap by characterizing them for different quasi-Fermi level splitting and hence defect states acting as recombination centers, obtained with different carrier generation rates. This is in agreement with the results first observed with the bulk recombination in solar cells, The differences that are present between the kinetics of relaxation in the photocurrents in the films and the recombination currents in cells can be attributed to those in the respective quasi-Fermi level splitting across the gap states around midgap acting as recombination centers. The two sets of results suggest that the densities of the states just above midgap are lower than those below. Another interesting result found is that in the relaxation after longer times of 1 sun illumination there is a systematic increase in the delays for the onsets of the logarithmic relaxations that nevertheless exhibit the same rates. This characteristic is also found to be consistent with the results on cells. To further address intriguing questions raised by these results on the nature and mechanism responsible for SWE studies are being extended to different temperatures as well as being carried out on different samples from the same depositions with their history being carefully controlled.

Light induced defect states and their energy distribution in a-Si:H films

Careful studies were carried out on the light induced defect states created by 1 sun illumination in diluted protocrystalline and undiluted a-Si:H films using the newly constructed dual beam photoconductivity (DBP) apparatus. Results are obtained which for the first time clearly identify *three* components in the energy distribution of light induced defects characterized by subgap absorption as well as the differences between the diluted and undiluted materials. Because of the extended photon energies to 0.5 eV it was also possible to characterize electron occupied states above midgap and to establish the presence of two distinct distribution of states close to midgap – one just above and the other just below. It is also found that the two Gaussian-like distributions of states below midgap are in agreement with those obtained from the n(V) characteristics of corresponding cells with the diluted protocrystalline and undiluted i-layers. The difference obtained in the relative densities of the states just above to those just below midgap are consistent with the results obtained for the room temperature relaxation of the photocurrents in films and the bulk recombination currents in cells. Furthermore, a room temperature relaxation has been observed in the states located around midgap after prolonged relaxation in the dark after 1 sun illumination.

Task 1: Materials Research and Device Development

The growth processes for a-$Si_{1-x}Ge_x$:H alloys have been investigated using RTSE. The goal is to develop deposition phase diagrams for the optimization of these materials for photovoltaic applications. In this quarter phase diagrams for $Si_{1-x}Ge_x$:H in the plane of d_b and R=[H_2]/{[SiH_4]+[GeH_4]} were found to exhibit detailed features similar to those of the previous diagrams for Si:H. First, an amorphous-to-(mixed-phase-microcrystalline) phase transition [a→(a+μc)] is observed that shifts to decreasing bulk layer thickness d_b with increasing H_2-dilution ratio R, thus opening up a protocrystalline growth regime. Second, an amorphous roughening transition (a→a) is observed that shifts to increasing d_b with increasing R up to the [a→ (a+μc)] transition. In this study, phase diagrams are explored for low power, low pressure $Si_{1-x}Ge_x$:H deposition as a function of temperature and electrode configuration. Low temperature (200°C) a-$Si_{1-x}Ge_x$:H depositions on the cathode with a self-bias of V_b ~ 20 V are promising in view of previous observations for optimum a-Si:H. These a-$Si_{1-x}Ge_x$:H depositions exhibit the largest a→a roughening transition thickness, up to ~ 2000 Å, when a high value of R ~100 just before the [a→(a+μc)] transition is used.

A comparison of the deposition rates for similarly-prepared a-Si:H and a-$Si_{1-x}Ge_x$:H is shown in Fig. 1. The only difference in the process is the replacement of 1/5 of the SiH_4 flow by GeH_4. The significantly higher rates for the alloys are attributed to the ease with which GeH_4 is dissociated in the plasma relative to SiH_4. Fig. 2 depicts the evolution of the surface roughness layer thickness with bulk layer thickness for selected $Si_{1-x}Ge_x$:H films with R=[H_2]/{[SiH_4]+[GeH_4]} = 15, 40, and 60 that remain amorphous throughout growth. Each of these films reveals an amorphous roughening transition, designated a→a because the film is purely amorphous on both sides of the transition. The results shown in Fig. 3 are for films with R=75, 80, and 100 that nucleate as a-$Si_{1-x}Ge_x$:H and exhibit an a→(a+μc) transition.

Fig. 4 shows the superimposed deposition phase diagrams for pure Si:H and for $Si_{1-x}Ge_x$:H alloy thin films, the latter deduced from the data of Figs. 2 and 3. Two significant differences are observed between the two diagrams, indicating the profound effect of alloying. First, the a→(a+μc) transition for the series of $Si_{1-x}Ge_x$:H alloys is shifted to much larger R compared to pure Si:H. Thus, the presence of Ge in the growth process appears to suppress the nucleation of microcrystals from the amorphous phase. Second, the a→a roughening transition for the $Si_{1-x}Ge_x$:H saturates at a low bulk layer thickness of 200 Å, even as the a→(a+μc) transition for thick films is approached and crossed. In contrast, for Si:H, the a→a roughening transition increases sharply, exceeding the bulk layer thickness of 4000 Å, as the a→(a+μc) transition is approached. This difference indicates that the diffusion length of precursors on the film surface during growth is significantly reduced for the alloys, likely due to surface defects that immobilize the precursors. Furthermore, it also suggests that no significant gain in the device performance of the alloys can be realized by increasing the H_2-dilution from R=40 to 70 [i.e., up to the a→(a+μc) transition for the bulk layer thickness desired in the device]. The reason for this latter suggestion is that the a→a transition thickness remains at its saturated value of ~200 Å throughout this range of R.

The effect of other deposition characteristics and parameters on the phase diagram was demonstrated, including substrate temperature and electrode configuration, in an attempt to increase the upper limit of the surface stability range to bulk layer thicknesses greater than 200 Å. In contrast to the case of pure Si:H, the broad range of R for a-$Si_{1-x}Ge_x$:H over which the a→a

transition thickness remains constant ($40 \leq R \leq 70$) suggests that, in elevating the temperature above 200°C, improvements can be made in the maximal R condition [that is, in spite of the expected shift to lower R in the a→(a+μc) transition]. This suggestion is borne out in the phase diagram for $Si_{1-x}Ge_x$:H prepared at T=290°C, shown in Fig. 5 for comparison with the corresponding diagram for $Si_{1-x}Ge_x$:H prepared at T=200°C. First, Fig. 5 reveals the expected shift in the a→(a+μc) transition to lower R (by ~20; i.e., a transition thickness of ~ 700 Å is shifted from R=80 to 60 with the substrate temperature increase). Second, with the increase in temperature, the a→a transition shifts to higher d_b from ~200 to 400 Å, indicating an enhancement in surface diffusion, and a modest improvement in material characteristics for solar cells.

Additional phase diagrams have also been developed for processes at 260°C and 320°C, as well as for a two step, 200°C/320°C process, the latter in order to enhance the nucleation density on the substrate and characterize the surface diffusion processes with greater confidence. Furthermore, a phase diagram versus temperature has been established for R=60. In these studies, under no temperature conditions has the a→a transition been found to exceed ~ 500 Å. Thus, having exhausted the potential of temperature increases to improve $Si_{1-x}Ge_x$:H surface stability under standard conditions, other less convention-al approaches were considered. On the basis of previous successes by Wickboldt et al. for a-Ge:H[1] and Ganguly et al. for a-Si:H[2], depositions were performed at T=200°C on the cathode of the reactor with a self-bias of ~ 20 V.

The deposition rates for the a-$Si_{1-x}Ge_x$:H prepared on the cathode and anode are shown in Fig. 6. The higher rates for the cathode series are related to higher gas dissociation rates due to more energetic ions crossing the cathode sheath. Fig. 7 depicts the dramatic differences in the microstructural evolution of R=80 $Si_{1-x}Ge_x$:H films deposited on the cathode and anode. The film deposited at the anode exhibits an a→(a+μc) transition at d_b = 700 Å and an a→a roughening transition at d_b = 200 Å; in contrast, the film deposited at the cathode remains amorphous throughout, exhibits a strong smoothening effect -- leading to a surface with d_s ~ 7 Å, and finally, exhibits a stable surface to a thickness of d_b~1500 Å.

Results such as those of Fig. 7 have been have been used to construct the phase diagram for cathode deposition in Fig. 8 shown along with the phase diagram for anode deposition from Figs. 4 and 5. This comparison reveals two important effects. First, a significant shift in the a→(a+μc) transitions to higher R is observed for deposition on the cathode versus anode. Second, the a→a transition shifts to larger thicknesses from 200 to 2000 Å for deposition on the cathode (relative to anode) as the a→(a+μc) is approached. Such behavior suggests significant improvement in the precursor surface diffusion under cathodic conditions. It is possible that low energy ion impact is sufficient to enhance the processes of H-elimination from the surface, leading to a more compact surface. The high H_2-dilution R > 60 then ensures a low defect density on the surface throughout this process.

[1]P. Wickboldt, D. Pang, W. Paul, J. Chen, F. Zhong, C.-C. Chen, J.D. Cohen, and D.L. Williamson, *J. Appl. Phys.* **81**, 6252 (1997).
[2]G. Ganguly, I. Sakata, and A. Matsuda, *J. Non-Cryst. Solids* **200**, 300 (1996).
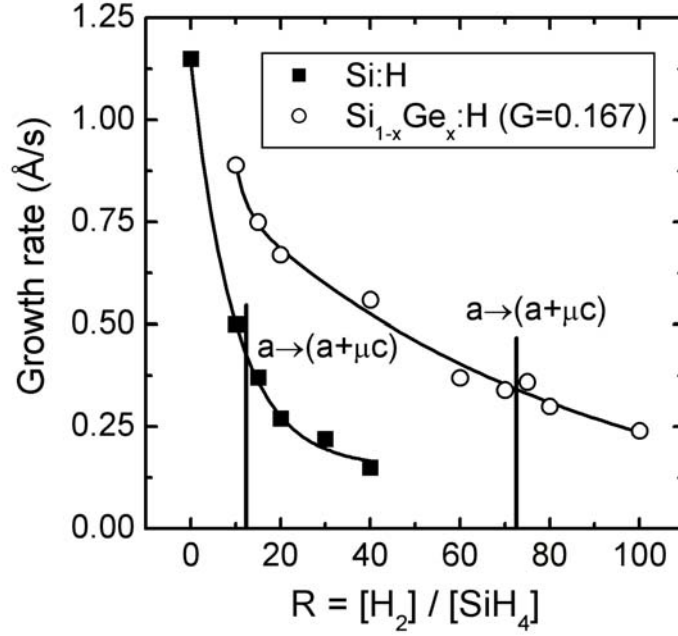
Fig. 1: A comparison of the deposition rates of pure Si:H and $Si_{1-x}Ge_x$:H films prepared as a function of the H_2-dilution ratio. For both series, the substrate temperature was 200°C, the plasma power was 0.08 mW/cm^2, and the reactive gas partial pressure was ~0.06 Torr.
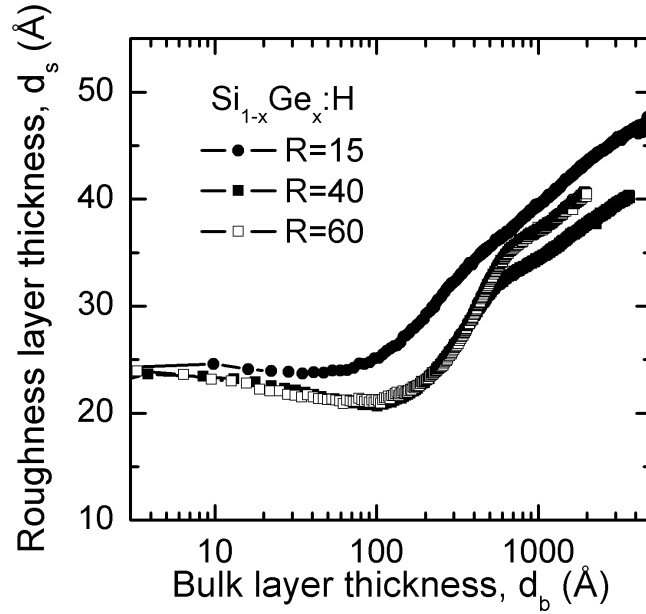
Fig. 2: Surface roughness layer thickness vs. bulk layer thickness for $Si_{1-x}Ge_x$:H films with R = 15, 40, and 60 that grow in the amorphous phase throughout deposition. For this series of films, the substrate temperature was 200°C, the plasma power was 0.08 mW/cm^2, and the reactive gas partial pressure was ~0.06 Torr.
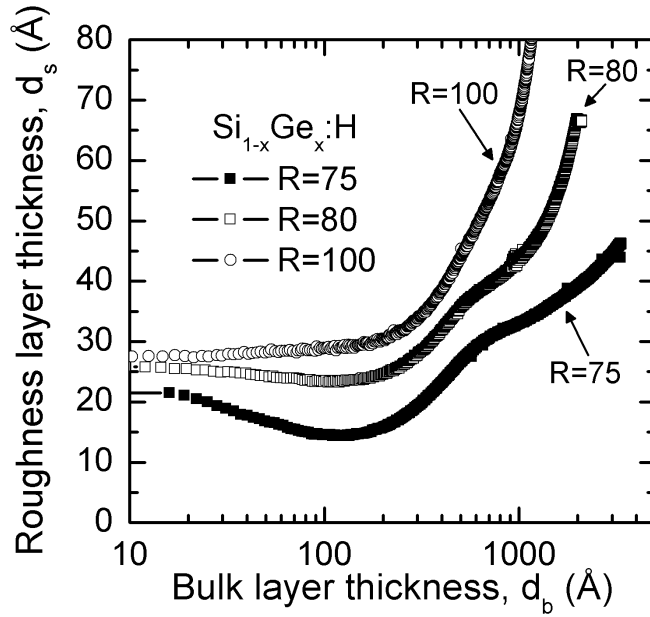
Fig. 3: Surface roughness layer thickness vs. bulk layer thickness for $Si_{1-x}Ge_x$:H films with R = 75, 80, and 100 that nucleate in the amorphous phase but evolve to the mixed-(amorphous+microcrystalline) phase with increasing thickness; other deposition parameters were the same conditions as those in Fig. 2.
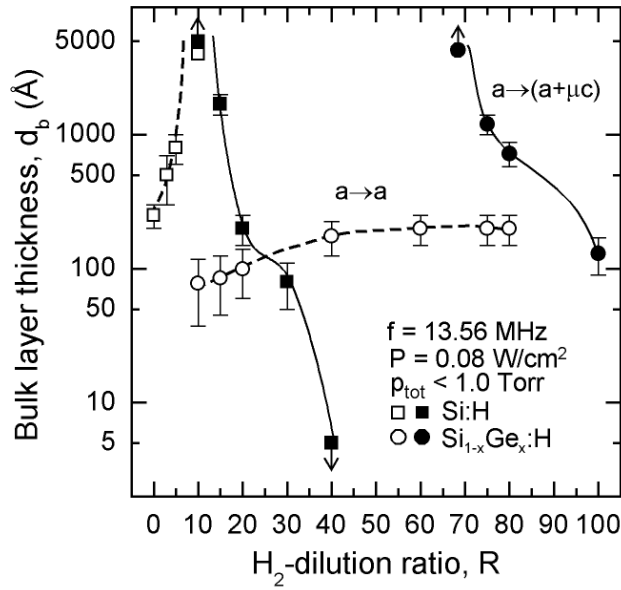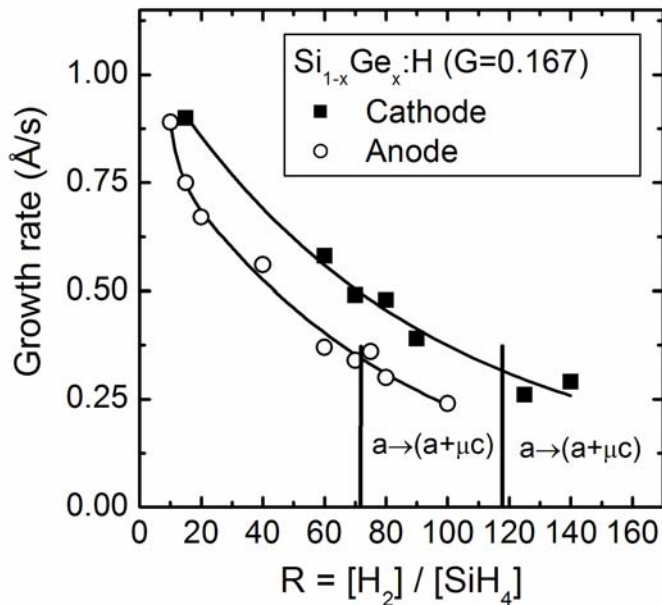

Fig. 4: Superimposed phase diagrams for Si:H (squares) and $Si_{1-x}Ge_x$:H (circles) films deposited at low power (0.08 mW/cm^2) and low total pressure (< 1 Torr) on native oxide-covered c-Si substrates held at 200°C. The (up, down) arrows indicate that the transition occurs (above, below) the designated value.
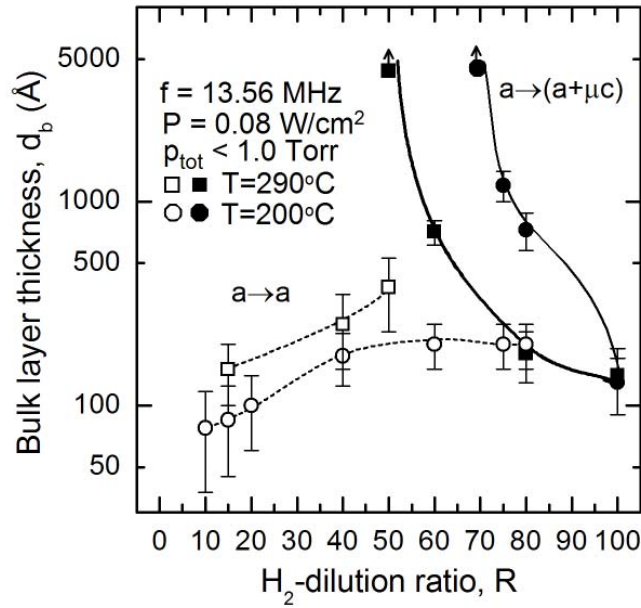
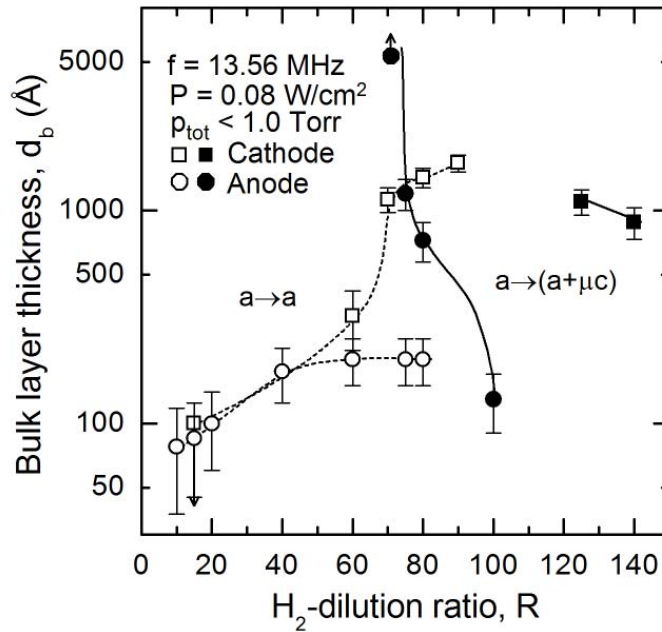**Fig. 5:** Superimposed phase diagrams for $Si_{1-x}Ge_x$:H films deposited under similar conditions at two different substrate temperatures (T=200°C and T=290°C). The temperature increase shifts the onset of the mixed phase transition to lower R, and generally results in an increased bulk layer thickness for the a$\rightarrow$ a transition.

Fig. 6: A comparison of the deposition rates of $Si_{1-x}Ge_x$:H films deposited on the cathode and anode prepared as a function of the H_2-dilution ratio R. For both series, the substrate temperature was 200°C, the plasma power was 0.08 mW/cm^2, and the reactive gas partial pressure was ~0.06 Torr.

9
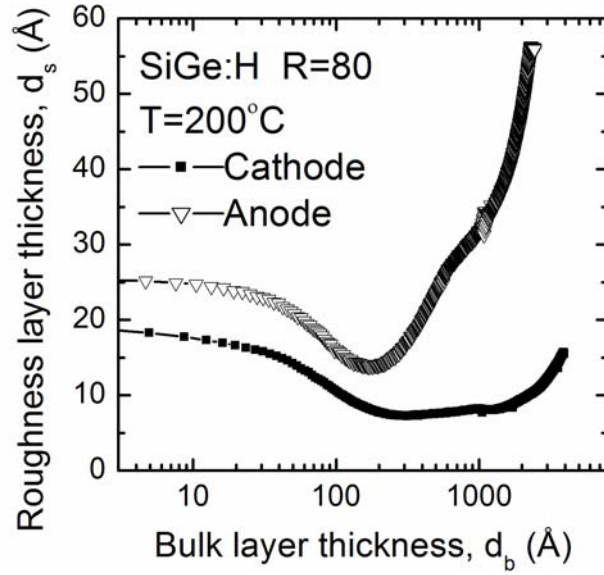
Fig. 7: Comparison of the structural evolution of $Si_{1-x}Ge_x$:H films deposited at the anode (triangles) and cathode (squares) using R=80 at low power (0.08 mW/cm^2) and low total pressure (< 1 Torr) on native oxide-covered c-Si substrates held at 200°C.

Fig. 8: Superimposed phase diagrams for $Si_{1-x}Ge_x$:H films deposited on the cathode (squares) and anode (circles) using oxide-covered c-Si substrates at 200°C.

Task 2: Device loss mechanisms

J_D-V characteristics have been utilized in addressing the limitations of bulk recombination on the 1 sun Voc's and the role of the different defect states in the i-layers of high quality solar cells. It has been shown that in the cells where bulk recombination dominates the current and the defect state distribution is essentially uniform across the bulk i-layer, there is a dependence of the J_D-V characteristics on the bulk i-layer thickness as a result of the scaling of the electric fields[3]. One natural extension to this is that because of the higher recombination in the thicker cells there should also be a corresponding reduction in their 1 sun V_{oc}'s. This requires that the bulk recombination dominates the carrier transport not only at relatively low biases but also at high biases up to 1 sun V_{oc}. That this is indeed the case has been found for cells with both protocrystalline R=10 and undiluted R=0 i-layers. This is illustrated in Fig. 9 which shows the results on the thickness dependence of 1 sun V_{oc} as well as J_D-V characteristics for p-i-n cells having the same structure but different thickness of R=0 bulk i-layers. In these cells the recombination at the p/i interfaces is minimized by having a 200Å of R=40 protocrystalline i-layer in the p/i region. It can be seen in the insert of Fig. 9 that the 1 sun V_{oc} decreases systematically with the increasing thickness of the bulk i-layer where a decrease of ~30mV (from about 0.89 to 0.86V) occurs in V_{oc} for an increase of a factor of 2 in the dark currents at low biases. This 30mV decrease in V_{oc} is consistent with the increase in the dark currents whose increase for this change in voltage corresponds to the "effective" diode quality factor of ~1.6 present in these cells[4]. It is important to note here that these V_{oc}'s were measured not with fixed illumination intensities but instead with a fixed J_{sc} of 10 mA/cm^2 (equivalent to 1 sun J_{sc} for the cells with 0.4μm thick i-layer) to eliminate the effect from the changes in light absorption due to the differences in the i-layer thickness. In thicker cells the increases in the dark current at voltages corresponding to 1 sun V_{oc} cannot be directly observed because they become limited by carrier injection over the potential barriers in the i-layers adjacent to the p and n contacts[3].

The domination of these V_{oc}'s by bulk recombination currents at biases corresponding to 1 sun V_{oc} in the cells studied could be further confirmed with the degradation kinetics of the 1 sun V_{oc}. Shown in Fig. 10 is the degradation of the 1 sun V_{oc} under 1 sun illumination at 25°C for the cell in Fig. 9 having the 0.4μm thick i-layer. It can be seen that there is an immediate decrease in the 1 sun V_{oc} that is a clear indication that there are no significant contributions from p/i interface recombination. After 100 hours of degradation there is a decrease in V_{oc} of around 50 mV that is consistent with the changes in the J_D-V characteristics of the same cell as shown in Fig. 11. In Fig. 11 there is an increase in the recombination current of a factor of ~3 at a bias that corresponds to the 1 sun V_{oc}.

Similar correlations between the degradation of V_{oc}'s and J_D-V characteristics are also obtained for the cells with R=10 protocrystalline i-layers. This is illustrated in Figs. 12 and 13 with results on a p-i-n cell with 0.4μm thick R=10 bulk i-layer and 200Å thick R=40 p/i interface. In Fig. 12 the decreases in V_{oc}'s measured under light intensities from 1 to 10^{-4} sun, are shown as a function of the degradation time under 1 sun illumination. It can be seen that as the light intensity and V_{oc} are lowered there are corresponding changes in both the rate and magnitude of the voltage decreases in reaching a degraded steady state after ~100 hours of illumination. For the illumination intensity of 10^{-4} sun, corresponding to an initial V_{oc} of 0.62V, there is a decrease of ~ 70 mV in V_{oc}. For 1 sun illumination the degradation is less than 10 mV,

[3] J. Deng, J.M. Pearce, R.J. Koval, V. Vlahos, R.W. Collins, and C.R. Wronski, *Appl. Phys. Lett.* **82**, 3023 (2003).
[4] J. Deng, J. M. Pearce, V. Vlahos, R. W. Collins, and C. R. Wronski, *Mater. Res. Soc. Symp. Proc.*, **808**, A8.8 (2004).

a value that is also significantly smaller than the 50 mV degradation of the 1sun V_{oc} for the cell with R=0 i-layer after the same degradation. This small degradation at such a high illumination level cannot be due to the limitations imposed by p/i interface recombination since a similar dependence of 1 sun V_{oc} on thickness was also found for the cells with R=10 i-layers. The degradation in V_{oc}'s in Fig. 12 can be directly correlated with the changes in J_D-V characteristics shown in Fig. 13. In Fig. 13 there are systematic increases in the dark currents with illumination time just as in the corresponding V_{os}'s. The changes in the currents, which are larger at the lower biases, correspond to the higher decreases in V_{oc}'s measured at the lower illumination intensities. Unlike the large change in the cell with the R=0 i-layer, there is hardly any discernable changes in the dark current at the levels equivalent to 1 sun J_{sc}. This cannot be completely due to the carrier injection limitations imposed by the potential barriers since these limitations occur at similar current levels for both types of the cells. The difference in the 1 sun V_{oc} degradation between the cells with the R=10 and R=0 i-layer thus clearly points to a distinct difference in their gap state distributions upon light induced degradation.

Several conclusions can be drawn from the above experimental results. First, in these cells the currents are dominated by bulk recombination up to bias levels equivalent to 1 sun V_{oc}. This is significant since then the results obtained on the J_D-V characteristics can be directly applied to the analysis of solar cell performance. Second, there are large light induced changes in the densities and distributions of the defect states in both the undiluted and diluted protocrystalline i-layers associated with Staebler-Wronski Effect (SWE). Thirdly, the distributions of gap states in the two i-layers are distinctly different, thus leading to the differences in the corresponding solar cell performance and stability.

In order to understand the relation between solar cell parameters such as V_{oc} and the distribution of gap states in the i-layers it is necessary to identify the differences present in the two i-layer materials. The essential features of the distributions for both the undiluted and diluted i-layers have been obtained from the analysis on the n(V) characteristics[5]. In both cases they are consistent with a Gaussian-like distribution around midgap followed by an exponentially rising distribution away from the midgap which could also be regarded as the rising edge of a second Gaussian-like distribution. Similar Gaussian-like distributions have been proposed in several previous studies[6]. There is however a major difference between the undiluted and diluted i-layer where in the former case the rising edge of the second Gaussian-like distributions are much less steep. Furthermore, after the introduction of light induced defects, the distributions in both i-layers broaden with a much smaller broadening occurring in the case of the protocrystalline i-layer. For both cases there is also a large increase in the density of states around midgap which causes the large increases in the dark currents under low forward biases and the large decreases in the V_{oc}'s under illumination intensities much smaller than 1 sun. However, in the case of the dark currents under high forward bias and V_{oc} under sufficiently high illumination intensity, the splitting between the two quasi-Fermi levels are sufficiently large as to include as recombination centers not only the gap states around midgap but also those located further away from the midgap. For the cell with protocrystalline i-layer, due to the narrower Gaussian-like distributions in the annealed and degraded states, the positions of quasi-Fermi levels at 1 sun V_{oc} are in a

---

[5] J. Deng, J. M. Pearce, V. Vlahos, R. W. Collins, and C. R. Wronski, *Mater. Res. Soc. Symp. Proc.*, **808**, A8.8 (2004).

[6] K. K. Mahavadi, K. Zellama, J. D. Cohen, and J. P. Harbison, *Phys. Rev. B*, **35**, 7776 (1987); L. Jiao, H. Liu, S. Semoushikina, Y. Lee, and C. R. Wronski, *Proc. 25th IEEE PVSC* (IEEE, New York, 1996), p. 1073; M. Günes and C. R. Wronski, *J. Appl. Phys*. **81**, 3526 (1997); V. Nadazdy and M. Zeman, *Phys. Rev. B*. **69**, 165213 (2004).

region where the native defects away from midgap play a dominant role in the recombination. This then explains the very small degradation of 1 sun V_{oc} while there is significant degradation for the V_{oc}'s under the lower intensities of illuminations. On the other hand, for the cell with undiluted i-layer, due to the broad distribution away from midgap the contribution from the light induced defects increases the recombination over that of the native defect states alone and accounts for the significant degradation in 1 sun V_{oc}. It is very important to note here that for cells having both undiluted and protocrystalline i-layers the degradation in the 1 sun V_{oc}'s are much smaller than that expected if these V_{oc}'s were limited purely by the recombination through the neutral dangling bonds, with states located around midgap and detected by electron-spin resonance. This is a further indication for the gap states other than the neutral dangling bonds determining cell performance[7] and the key role of the Gaussian-like distributions away from midgap identified from the analysis of the n(V) characteristics.

---

[7] B. Von Roedern, *Appl. Phys. Lett.* **62**, 1368 (1993); J. Pearce, X. Niu, R. Koval, G. Ganguly, D. Carlson, R. W. Collins, and C. R. Wronski, *Mater. Res. Soc. Proc*. **664**, 1231 (2001).
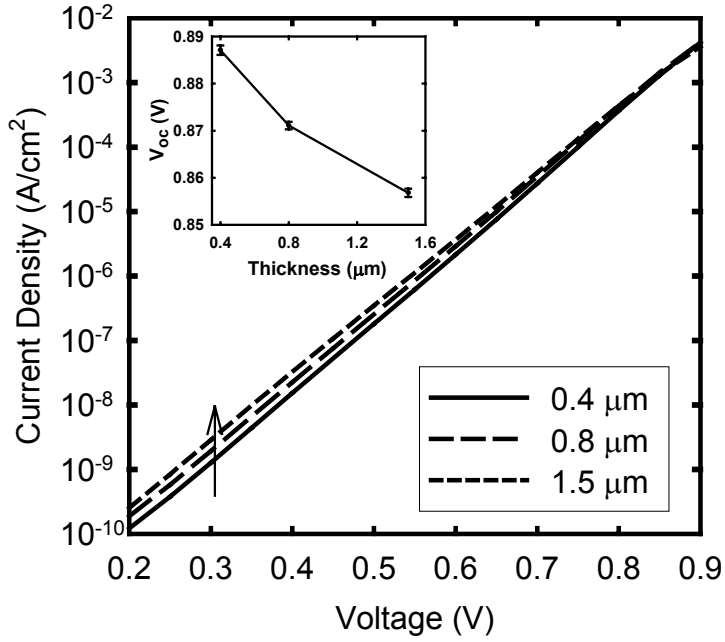
Fig. 9: Thickness dependence of 1 sun V_{oc} and J_D-V characteristics for p-i-n cells having the same structure but different thickness of R=0 bulk i-layers.
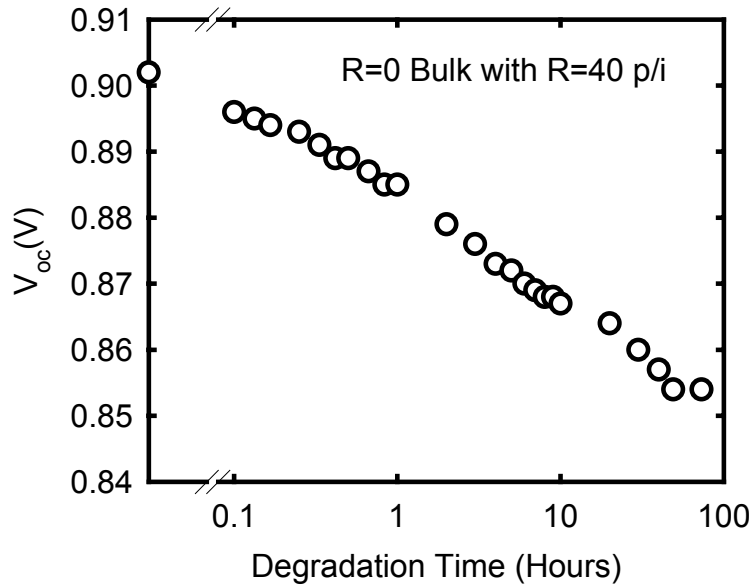

Fig. 10: Degradation of 1 sun V_{oc} under 1 sun illumination at 25°C for the cell in Fig. 9 with the 0.4μm thick i-layer.
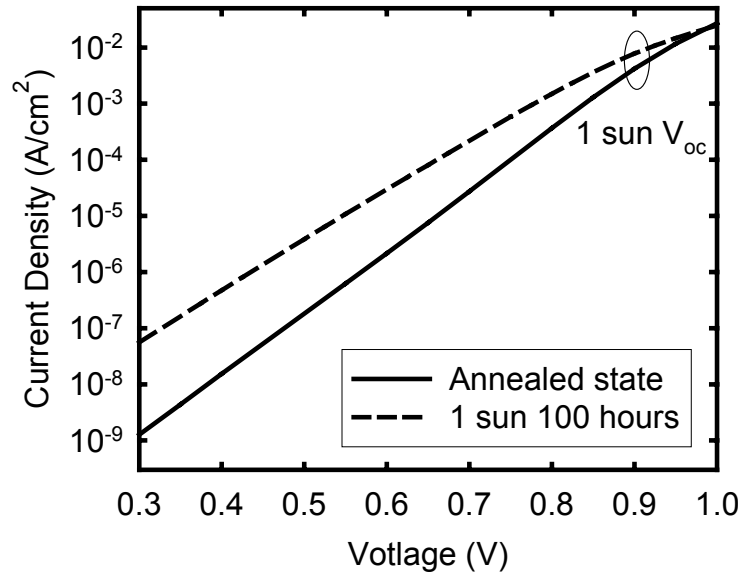
Fig. 11: J_D-V characteristics of the cell in Fig. 10 in the annealed state and after 100 hours of 1 sun illumination.
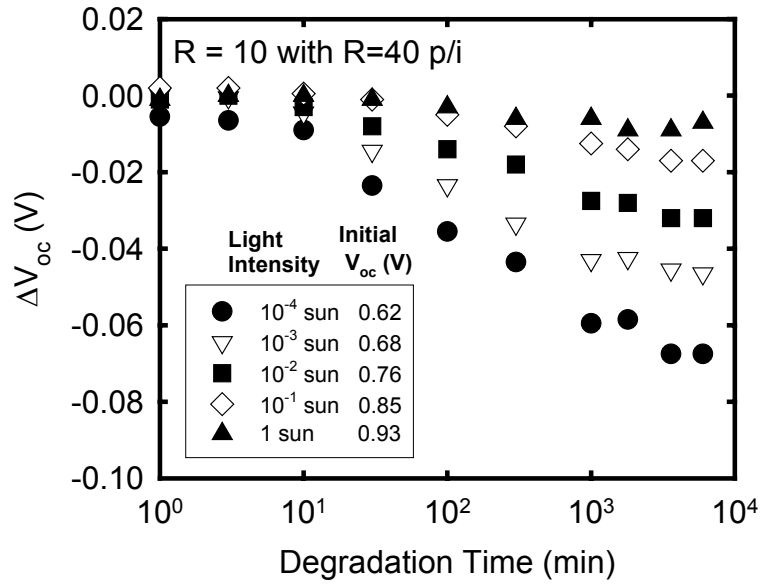
Fig. 12: Degradation of V_{oc}'s for a p-i-n cell with 0.4μm thick R=10 bulk i-layer and 200Å thick R=40 p/i interface measured under light intensities from 10^{-4} to 1 sun.
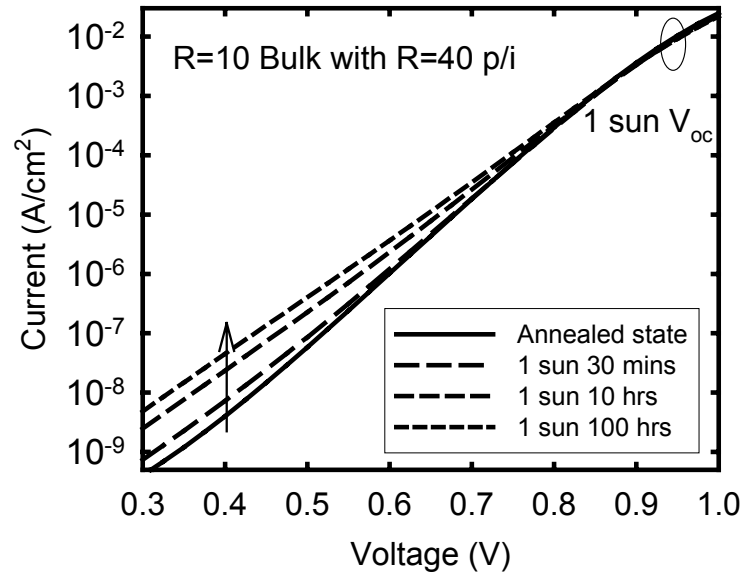
Fig. 13: J_D-V characteristics of the cell in Fig. 12 in the annealed state and after light induced degradation.

Task 3: Characterization Strategies for Advanced Materials

Room temperature changes in light induced defect states created by 1 sun illumination

The kinetics of 1 sun light induced degradations in this study were monitored not only with 1 sun photocurrents, as is generally done, but also with uniformly absorbed probe illumination with carrier generation rates, G, of 10^{15} to 10^{18} cm^{-3}s^{-1}. Such probes were subsequently used in characterizing the recovery of photocurrents having different generation rates after the films were exposed for different times to 1 sun illumination. Very good reproducibility was obtained for the degradation kinetics and values of the photocurrents for the same extended times of illumination after intermediate experiments and annealing of 170 $^{\circ}$C for four hours. The variations that exist in the first few minutes of 1 sun illuminations are a result of the fast changes[8] and are attributed to surface band bending associated with the film interfaces. This is eliminated by either the fast creation of donor or elimination of acceptor states with 1 sun illumination. In the course of the detailed studies a given degraded state was found to depend on its history. After multiple degradation and anneals reproducibility within 10% is obtained in the 1 sun and probe degraded photocurrents. There is a systematic change in the first of the two rates observed in the photocurrent relaxation. This is illustrated in Fig. 14. These results were obtained after 1 sun illumination of 30 minutes at different stages of the investigations and show the changes in the recovery of the normalized photocurrents as a consequence of intermediate experiments. In Fig. 14 the open symbols are for G= 1×10^{15} and the filled symbols for 1×10^{16}. A systematic increase in the delay before the photocurrents increase logarithmically with time can be seen in Fig. 14, but despite this the corresponding rates remains essentially the same. This would suggest that there are two types of defect states located close to midgap.

The dependence of the photocurrent relaxation on the generation rate, and hence the quasi-Fermi level splitting, shows that the most rapid changes occur when the recombination is dominated by the states closest to midgap. This can be seen from the systematic decreases in the logarithmic rates of relaxation as the quasi-Fermi levels move further and further away from midgap and additional states act as recombination centers. This is illustrated in Fig. 15, which shows the results for photocurrents with increasing carrier generation rates for generation rates of 1×10^{15} to 4×10^{17} cm^{-3}s^{-1} where the position of the electron Fermi level is moved from 0.64 to 0.57 eV from E_c respectively. In Fig. 15 the reciprocal of the photocurrents normalized to their initial values are plotted as a function of time to exhibit that the photocurrents dependence on the inverse of the densities of such states. The results in Fig. 15 are consistent with the J_D-V characteristics for the recombination currents in the bulk of the i layers of corresponding p-i-n solar cells shown in Fig. 16. Fig. 16 shows the normalized recombination currents after 30 minutes of 1 sun illuminations obtained for forward biases of 0.3, 0.4, and 0.5 volts. In this case the forward bias voltage determines the quasi- Fermi level splitting and these currents are proportional to the densities of states acting as recombination centers. In comparing the two sets of results it should be noted that there is a difference between the recombination being characterized in the two cases.

In the case of the film photocurrents the quasi-Fermi levels are determined by the densities of electrons and holes so that due to the higher densities of electrons the quasi-Fermi level for holes is closer to midgap. As a consequence more of the states above midgap than

---

[8] L. Jiao, H. Liu, S. Semoushikina, Y. Lee, and C. R. Wronski, *Appl. Phys. Lett.* **69**, 3713 (1996).

below are introduced as recombination centers so they play a more important role in the kinetics of relaxation. On the other hand in the case of the cells, the quasi-Fermi levels split symmetrically about midgap so there is an equal introduction. The results in Figs. 15 and 16 are consistent with an asymmetry in the densities of these states with a higher density of those just below midgap, which leads to a difference in the rates of relaxation.

Results were also obtained for degraded states after different degradation times. In Fig. 17 results are shown for the relaxation of the inverse of the normalized photocurrents with G= 10^{16} cm^{-3} s^{-1} after 1 sun illuminations. It is seen that as the illumination time increases so does the onset of the logarithmic relaxation rates that essentially remain the same. These characteristics are also present in the results on the p-i-n cells as seen in Fig. 18 where the normalized recombination currents for 0.4V forward bias are shown after 30 minutes, 10 hours, and 100 hours of 1 sun illumination. The similarity between these results and those characterizing the effects associated with the history of the degraded state suggests that there is a connection between the two.

This study on the "fast" states raises intriguing questions about their nature and origin as well as the results that are obtained for nominally "identical" degraded states.

Light induced defect states and their energy distribution in a-Si:H films

Dual Beam Photoconductivity (DBP) subgap absorption studies were carried out on dilute protocrystalline R=10 and undiluted R=0 thin films, 0.8-1.0 μm thick, with photon energies from 2.0 to 0.5 eV on the system previously described in the Phase II annual report.The enhanced sensitivity and energy resolution of the new DBP system allowed the energy distribution of the electron occupied states to be better characterized. The extension of the photon energies to 0.5 eV allowed states above midgap to be investigated. The subgap absorption, $\alpha(h\nu)$, was measured over a range of bias illuminations, and hence displacements of the quasi-Fermi levels, that were maintained constant for the different degrees of 1 sun degradation at 25°C. The generation rates used were sufficient to suppress any significant contributions of the room temperature relaxation discussed in the previous section during the time necessary to obtain the total $\alpha(h\nu)$ spectra (approximately 15 minutes). The distributions of the electron occupied states, N(E), from such spectra were obtained with the relation $\alpha(h\nu)$ by: $kN(E) = d(\alpha(h\nu))/d(h\nu)-\alpha(h\nu)$[9] where k is a constant optical matrix element for electron transitions from the different gap states into the conduction band. Excellent reproducibility in the $\alpha(h\nu)$ spectra was obtained where this is illustrated in Fig. 19 after FFT obtained on a R=10 film after 30 minutes of 1 sun illumination with intermediate experiments and annealing at 170°C for 4 hours having been carried out. In Fig. 20 are shown the kN(E) spectra obtained immediately after a 1 sun exposure for 30 minutes for films deposited under the same conditions with hydrogen dilution ratio R=10 and R=0. These spectra have been normalized to the densities of states at the valence band edge of 3×10^{21} cm^{-3} eV^{-1}with a subsequent displacement of 60 meV to take into account the difference in their bandgap. For the *first time* not only are three distinct distributions of states in a-Si:H films identified but also the presence of two in the close proximity to midgap – one just above and the other just below midgap. There is also a clear asymmetry between the densities of these two states, with those just above midgap being lower

---

[9] PSU NREL Annual Report, 2003

than those just below and ratios that are distinctly different in the two materials. It is also evident, as has been established from the results of the n(V) characteristics of corresponding solar cells and discussed in Section 2, the two Gaussian-like distributions below midgap are significantly narrower in the R=10 than in the R=0 material It is important to note also that this asymmetry between the two densities of states close to midgap is consistent with that proposed in explaining the differences in the relaxation kinetics due to different quasi-Fermi level splitting present in the photocurrent and cell recombination currents.

Relaxation in the gap states around midgap was found only after extended periods of relaxation in the dark because of the intentional suppression of the initial relaxations with the bias illumination. The results obtained for an R=10 film are shown in Fig. 21 which shows the kN(E) spectra obtained immediately after a 30 minute light exposure to 1 sun illumination and after 15 hours of relaxation in the dark. A marked decrease in the electron occupied states around midgap can be clearly seen in Fig. 21, which is in agreement with the results obtained for both the photoconductivity results on the films and J_D-V characteristics on cells.

The evolutions in the kN(E) spectra with time of 1 sun illumination are being further investigated as well as their dependence on the quasi-Fermi splitting obtained with different bias illuminations. Analysis based on the presence of Gaussian-like distributions is being related to the corresponding results obtained from the n(V) characteristics of solar cells in order to establish self-consistent interpretations about the nature of these states.
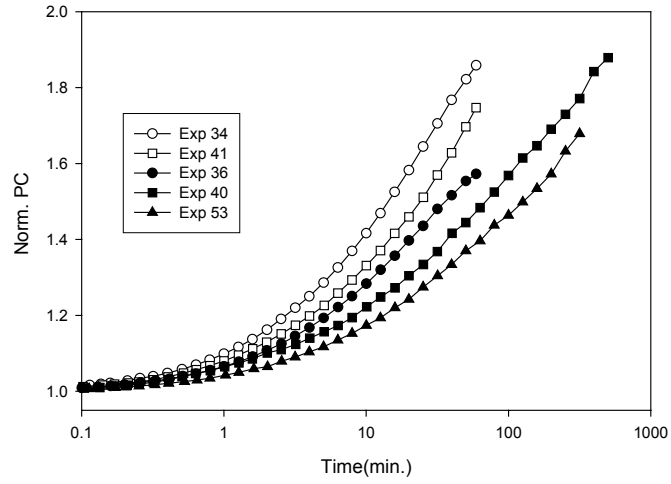
Fig. 14: Relaxation of the normalized photocurrents from nominally the same degraded states after 30 minutes of 1 sun illumination. Open, closed symbols for G of $1x10^{15}$ and $1x10^{16}$ respectively.
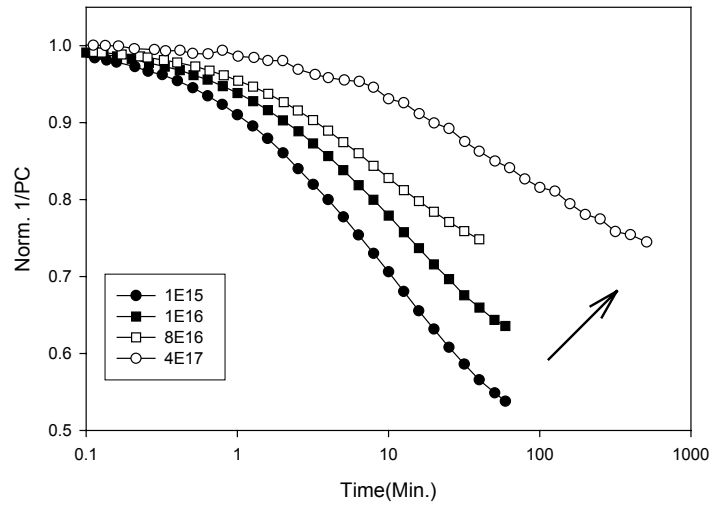

Fig. 15: Relaxation of the inverse normalized photocurrents for different G with increasing Quasi-Fermi level splitting indicated by the arrow in the figure.
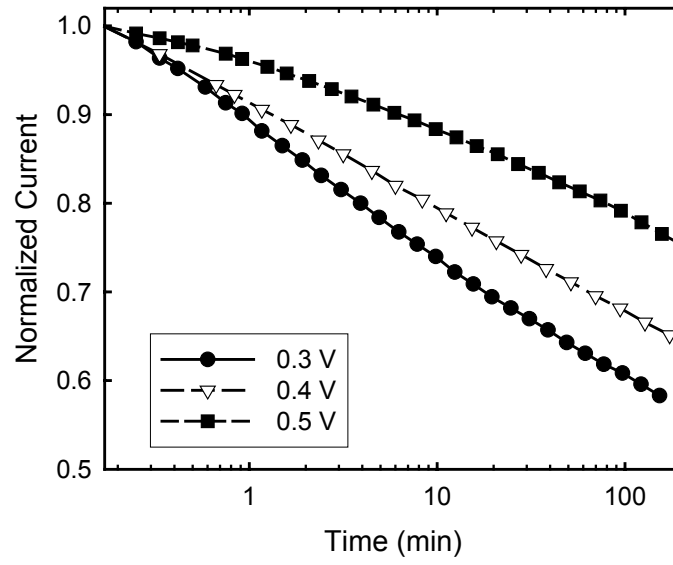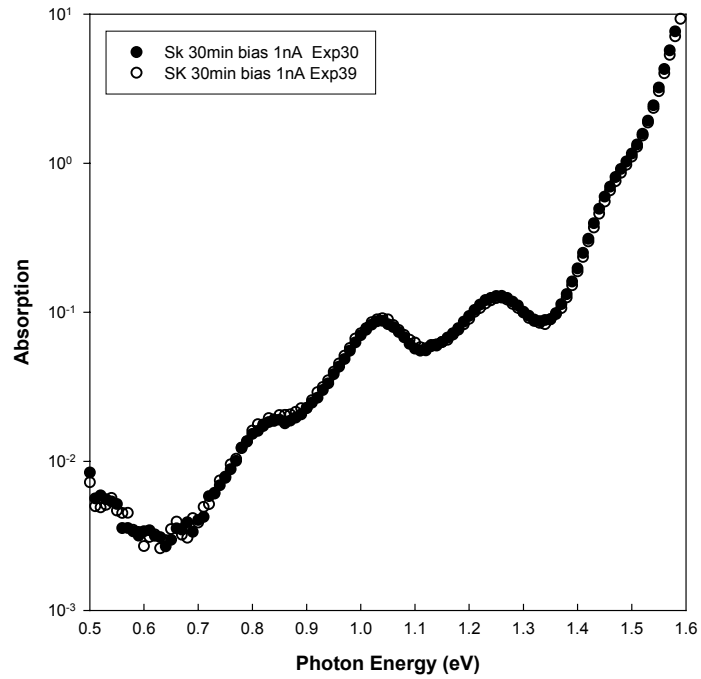
Fig. 16: Normalized recombination currents after 30 minutes of 1 sun illuminations obtained for forward biases of 0.3, 0.4, and 0.5 volts.
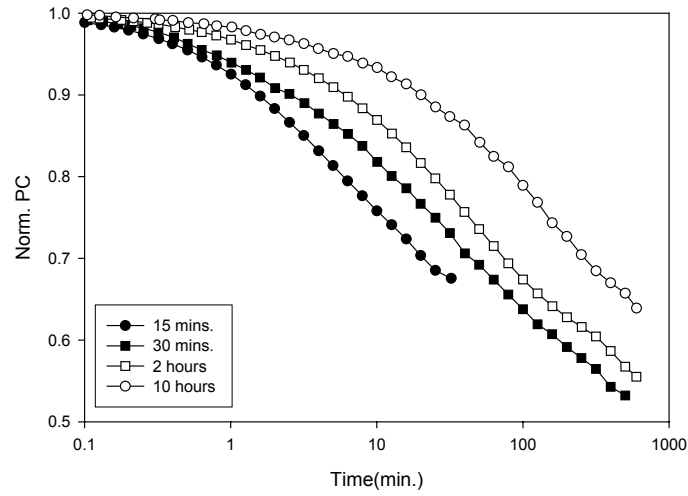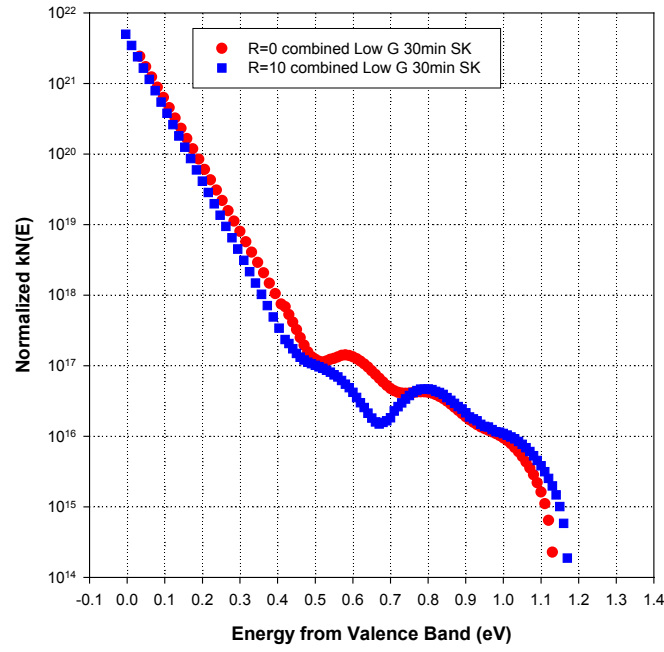

Fig. 17: Normalized inverse photocurrents after different times of 1sun illumination for $G=1\times10^{16}$.
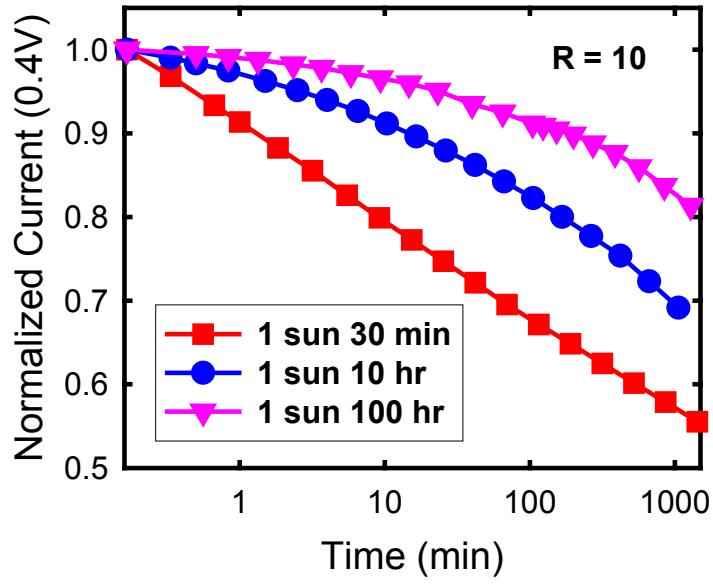
Fig. 18: Normalized recombination currents for 0.4V forward bias after 30 minutes, 10 hours, and 100 hours of 1 sun illumination.

Fig. 19: Scans for subgap absorption obtained after 30 minutes of 1 sun illuminations in two separate experiments.

Fig. 20: The kN(E) spectra for an R=10 and R=0 film after 30 minutes of 1 sun illumination normalized to the densities of states at the valence band edges.
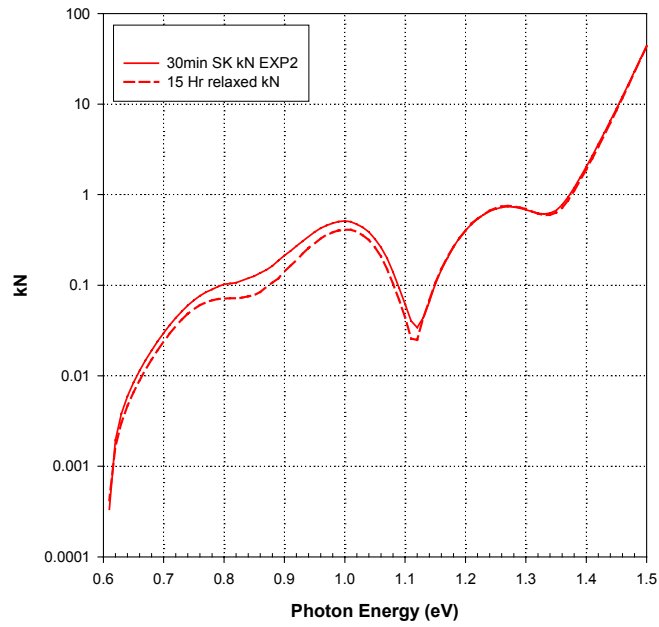
Fig. 21: The kN(E) spectra for an R=10 film immediately after 30 minutes of 1 sun illumination and after relaxation in the dark for 15 hours.